



Fractional-order creep model for soft clay under true triaxial stress conditions

Liu Jiashun^{1,2,3} · Jing Hongwen² · Meng Bo² · Wang Laigui³ · Yang Jianjun¹ · You Yanwei¹ · Zhang Sijin¹

Received: 3 September 2019 / Accepted: 12 August 2020 / Published online: 21 August 2020
© Saudi Society for Geosciences 2020

Abstract

To investigate the creep characteristics of soft clay under true triaxial stress conditions, multistage loading creep tests using TSW-40 true triaxial apparatus were performed. The creep deformation characteristics, creep rate, and long-term strength of soft clay under a true triaxial stress path were studied. The results showed that the creep deformation and creep rate of soft clay increase with increasing major principal stress; the axial deformation is larger than the lateral deformation. The long-term strength and the equation for predicting the starting point of accelerated creep were obtained using the generalized shear stress. A four-element fractional-order creep (FFC) model based on the fractional Burgers creep model was established for soft clay and then extended to three dimensions. The model calculation results based on the parameters obtained using MATLAB's Curve Fitting Toolbox were in good agreement with the experimental results. The comparison results showed that the 3D FFC model was more accurate at describing the entire creep curve of soft clay than the fractional Burgers model and the Burgers model, particularly regarding the accelerated creep characteristics. In conclusion, the results presented herein are expected to provide the scientific basis for determining soft clay creep instability under true triaxial stress conditions.

Keywords Soil mechanics · Soft clay · True triaxial stress test · Burgers model · Fractional-order model · Creep deformation

Introduction

Soft clay presents unique rheological properties that can easily cause foundation instability, landslides, or other geotechnical problems. Therefore, research on the creep characteristics of soft soil is very important to ensure the safety of the engineering. However, most previous geomaterial research is based on conventional triaxial stress conditions, whereas the majority of soils in practical engineering applications experience complex triaxial stress conditions; thus, their mechanical

characteristics and failure behaviors differ significantly from those in the 1D or 3D stress states (Isakhanov 2000; Liu and Shao 2018). So far, many true triaxial tests were performed to investigate the influence of intermediate principal stress on the stress–strain and strength behavior of clays and sands (Shao and Luo 2011; Shi et al. 2011). An empirical equation of $g(b)$, a shape function of the failure surface on π -plane, was presented and verified based on the true triaxial test results (Shi et al. 2010). A 3D anisotropic failure criterion is proposed to describe the strength of cross-anisotropic sands under true triaxial conditions, and the influence of the anisotropic parameter on the failure curve on the deviatoric plane and the relationship between the peak friction angle and the intermediate principal stress ratio are obtained. The coupled fluid-discrete element method is used to simulate the undrained response of initially anisotropic particulate assemblies under true triaxial condition (Salimi and Lashkari 2020). Many studies also have shown that the intermediate principal stress coefficient has a significant effect on the strength and deformation of geotechnical materials (Lv et al. 2011; Shi et al. 2015; Kumruzzaman and Yin 2010); the strength criterion for coarse-grained soil has previously been established according to this coefficient. Moreover, research has shown that complex stress states affect

Responsible Editor: Zeynal Abiddin Erguler

✉ Liu Jiashun
liujiashun000@163.com

¹ College of Civil Engineering, Liaoning Technical University, Fuxin 123000, China

² State Key Laboratory for Geomechanics and Deep Underground Engineering, China University of Mining & Technology, Xuzhou 221116, China

³ School of Mechanics and Engineering, Liaoning Technical University, Fuxin 123000, China

the anisotropic deformation and shear strength characteristics of marine soft clay (Hajime et al. 2002; Morsy et al. 1995; Wang et al. 2016; Xu et al. 2017).

The appropriate creep constitutive model can accurately and quantitatively describe the effects of creep, strain rate, and stress relaxation on the deformation and strength characteristics of soft clay and also can predict the development of soft soil deformation in the engineering project. Therefore, an accurate rheological model is significant important (Gupta 1978; Hao et al. 2019; Kuhn and Mitchell 1992; Zhan et al. 1993). Researchers have put forward many kinds of rheological constitutive models for soft clay, which mainly include empirical models, component models, and viscoelastic plastic mechanical models (Morsy et al. 1995; Nadimi and Shahriar 2014; Yin et al. 2002; Zhao et al. 2004). The component combination models, which are based on profound theoretical basis, have strictly mechanical processes and present parameters with clear physical meanings. Thus, component combination models have been widely used for the investigation of the rheological properties of geomaterials. However, there are still some defects in the integral order element combination model in describing the unsteady creep characteristics of soft soil, such as the lack of describing ability, etc., and the existing element combination model needs to be improved.

Fractional calculus theory, which can analyze different arbitrary orders, effectively describes the rheological properties of geomaterials and the evolution of the system structural features (Xu and Jiang 2017; Zheng and Wen 2013; Zhou et al. 2011). The fractional-order Maxwell model, fractional-order Burgers model, elasto-viscoplastic damage creep model, and variable order fractional constitutive model are all examples of models based on the fractional calculus theory (Hanyga 2007; Mainardi 2010; Wu et al. 2014; Zhou et al. 2011). The fractional-order creep model has been used to describe the rheological properties of mudstone, frozen soil, and fractured rock (Chen et al. 2015; Li et al. 2013) and has been proposed for describing the creep behavior of coral sands (Sun and Cheng 2018). Therefore, the fractional element model has great potential in describing the rheological properties of soft soil. Therefore, the long-term strength, creep deformation, and creep constitutive model of soft clay under true triaxial stress conditions are important for the stability of soft clay engineering. However, the creep properties of soft clay under true 3D stress path had not yet been researched well.

Above all, the multistage loading creep tests of soft clay under a true 3D stress path are performed using the TW-40 apparatus in this paper. Then, the creep deformation

characteristics, instantaneous deformation, and creep rate changes of soft clay are tested under different generalized shear stresses. A four-element fractional-order creep model (FFC model) for soft clay is established based on the fractional Burgers model, and then extended to the 3D state. Finally, the sensitivity of the parameters and the accuracy of the model are analyzed. The research results can be widely employed for engineering practices, especially for the creep behavior of soft clay under true triaxial stress conditions.

True triaxial creep tests of soft clay

Soil samples

The soil samples used in this experiment were taken from Fuxin Station on the Beijing to Shenyang Passenger Railway Line. The soil samples were obtained by digging to approximately 1.5 m depth after removing corrosive surface substances. The physical and mechanical parameters of the collected soft clay were determined and the parameters are presented in Table 1. Particle size analysis revealed that approximately 25–35% of the particles presented sizes from 0.075 to 1 mm and approximately 50–60% of particles were smaller than 0.075 mm. Therefore, the soil was classed as silty clay.

Test procedure

TSW-40 true triaxial soil test apparatus was used in the experiment. Firstly, the specimen was saturated using the vacuum saturation method. Then, the specimen was loaded into the pressure cell and precompacted. The major principal stress (σ_1), intermediate principal stress (σ_2), and minor principal stress (σ_3) were applied simultaneously at a loading rate of 0.01 kN/min. Loading was stopped when the three principal stresses reached 100 kPa and the specimen was isotropically consolidated. The σ_1 and σ_2 stresses were then applied continually to 110.5 kPa while maintaining a constant confining pressure of 100 kPa, at which the consolidation degree reached 95%. Then, σ_1 was applied to 120.9 kPa while keeping σ_2 and σ_3 constant. At this point, the initial intermediate principal stress coefficient, $b_0 = (\sigma_2 - \sigma_3)/(\sigma_1 - \sigma_3)$, reached the predetermined value of 0.5. The rheological tests were then initiated immediately.

Table 1 Physical and mechanical properties of soft clay

Density/g cm ⁻³	Moisture contents (w)/%	Plasticity index (I_p)	Cohesion (c)/kPa	Void ratio (e)
1.76	34.8–41.6	11.6–12.8	5.1–15.3	0.78–0.93

The rheological medium exhibits a memory effect of the loading history. Thus, the rheological curves of soft clay under different stress levels can be obtained using the linear adding principle theory. The major principal stress (σ_1) values were 120.9, 141.8, 162.9, 184.1, 204.6, and 225.8 kPa, respectively, and the corresponding intermediate principal stress coefficient (b) values were 0.5, 0.25, 0.17, 0.12, 0.10, and 0.08. The load of each stage lasted approximately 50 h and the total test time was approximately 280 h.

Creep test analysis

Strain results

The creep test results are shown in Fig. 3. The major principal strain (ϵ_1) of soft clay is larger than the minor principal strain (ϵ_3) and intermediate principal strain (ϵ_2) under true triaxial stress conditions; the values of ϵ_1 , ϵ_2 , and ϵ_3 when the samples fail or reach the failure criteria were 3.568%, -0.5742%, and 1.983%, respectively. The axial deformation is larger than the lateral deformation; ϵ_3 is larger than ϵ_2 because the ϵ_3 direction is a flexible constraint, while the ϵ_2 direction is a semi-rigid and semiflexible constraint. The failure mode involves axial compressive deformation and lateral dilatation deformation (Fig. 1).

The creep test results for soft clay show that no accelerated creep occurs when $\sigma_1 < 184.1$ kPa. In general, creep curves exhibit deceleration creep and steady creep when $\sigma_1 < 141.8$ kPa; this corresponds to a superstable creep state in which the creep rate approaches 0. However, the creep rate of the steady creep curve is not 0 and increases at a large constant rate when σ_1 is between 141.8 and 184.1 kPa; this corresponds to a metastable creep state. Accelerated creep tends to occur in the late loading stage if $\sigma_1 \geq 184.1$ kPa.

However, the major principal strain (ϵ_1) only reaches 4.625%, which is below the test failure criterion ($\epsilon_1 = 8\%$). Therefore, the next stage load is applied, where σ_1 is 225.8 kPa. After loading for approximately 11.35 h, accelerated creep begins to occur in the specimens; creep failure occurs until approximately 23.35 h of loading. Therefore, the creep constitutive model of soft clay should consider the instantaneous deformation, deceleration creep, constant rate creep (steady creep), and accelerated creep characteristics of the soil.

Analysis of instantaneous and creep deformation

The instantaneous elastic characteristics of soil are important indices of its strength and the creep characteristics of soil determine its stability. Instantaneous elastic deformation of soft clay occurs at the start of loading; then creep deformation occurs when the load becomes constant. The instantaneous deformation was taken as the values of the initial deformation, and creep deformation was obtained by subtracting the total deformation from the instantaneous deformation. Figure 2 shows the relationship between instantaneous and creep strain and the major principal stress (σ_1). Creep strain is always larger than the instantaneous strain, and the ratio of creep strain to instantaneous strain increases with increasing major principal stress, i.e., ϵ_1/ϵ_{1s} is 2.56, 3.21, 3.44, 4.37, 5.68, and 12.53 when σ_1 is 120.9, 141.8, 162.9, 184.1, 204.6, and 225.8 kPa, respectively. Similarly, ϵ_2/ϵ_{2s} vs. σ_1 and ϵ_3/ϵ_{3s} vs. σ_1 exhibit the same trend, which indicates that creep deformation increases with increasing loading stress. Thus, creep instability failure caused by increased loading plays a significant role in soft clay deformation and should be fully considered in design and construction applications.

Fig. 1 Creep test results for soft clay

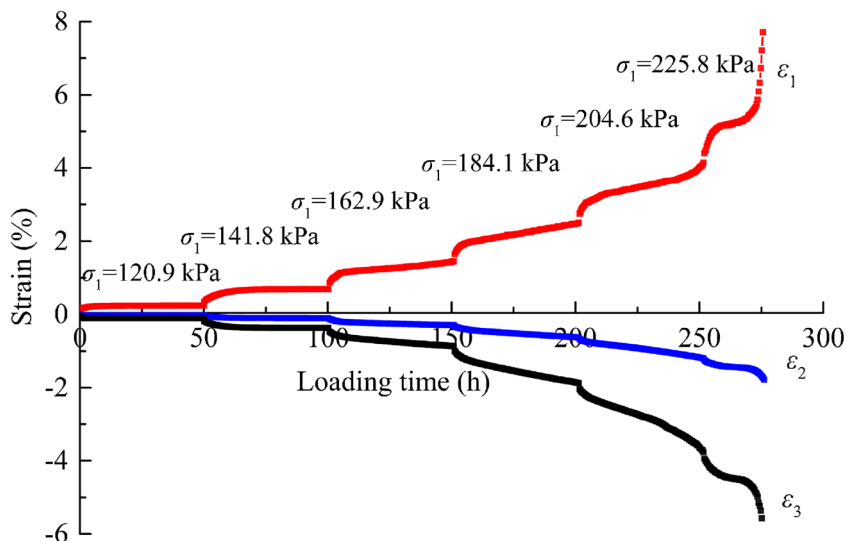
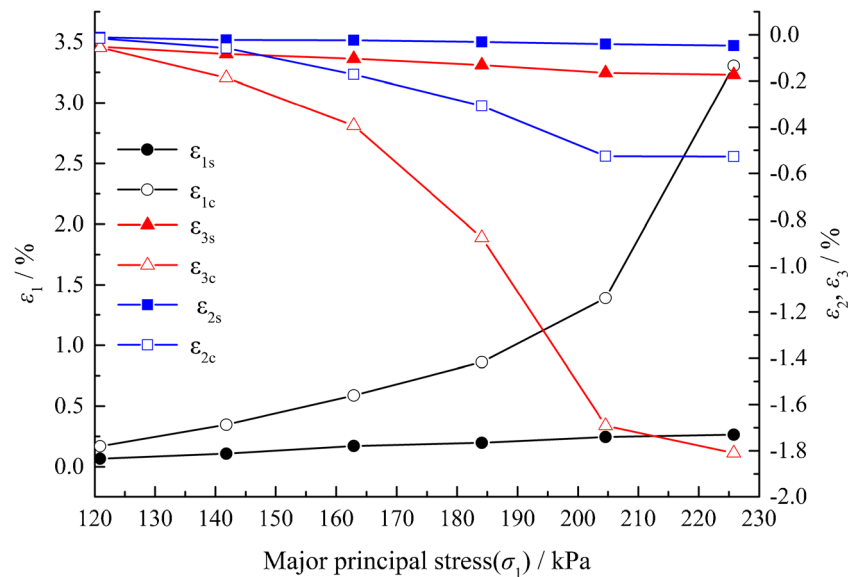


Fig. 2 Instantaneous strain and creep strain results for soft clay. ε_{1s} —major instantaneous strain, ε_{2s} —intermediate instantaneous strain, and ε_{3s} —minor instantaneous strain; ε_{1c} —major creep strain, ε_{2c} —intermediate creep strain, and ε_{3c} —minor creep strain



Analysis of creep rate

The creep rate can be used to determine the variability of creep deformation and predict the stability of soil or engineering structures. Herein, the creep rate curves were obtained by deriving the first-order of the creep test result, as shown in Fig. 3. The strain rate is higher at the moment of loading, which corresponds to instantaneous deformation of the specimen. The creep rate then decreases continuously, which corresponds to the deceleration creep stage. The duration of deceleration creep is 9.143, 8.403, 8.024, 7.983, 6.303, and 3.361 h when σ_1 is 120.9, 141.8, 162.9, 184.1, 204.6, and 225.8 kPa, respectively; thus, deceleration creep decreases with increasing major principal stress. This indicates that σ_1 significantly affects the duration of deceleration creep and that the constant creep state of soft clay should be considered in practical engineering design and construction. Consequently, this paper considers the duration and stress conditions of constant creep.

The stage at which the creep rate remains constant is called the constant creep stage. The constant creep state duration values for soft clay at the above major principal stresses are 42.857 h, 41.597 h, 41.176 h, 40.336 h, 35.297 h, and 14.706 h, respectively. These values were derived by extracting the corresponding time points at which accelerated creep occurred or those at the end of loading and the end of deceleration creep. In general, lower loads result in longer constant creep and deceleration creep duration values.

The creep rate of soft clay increases when σ_1 is 204.6 kPa at a loading time of 41.604 h and when σ_1 is 225.8 kPa at a loading time of 18.067 h; accelerated creep of the specimen occurs at this time. However, the cumulative axial creep strain of the specimens is 4.14%, which does not meet the 8% failure criterion stipulated in this study when σ_1 is 204.6 kPa and the loading time is 50 h; therefore, the next load is applied. The axial strain of the specimen reaches

7.7% when σ_1 is 225.8 kPa and the loading time is 23.529 h, indicating creep failure of the specimen and the end of the test.

Long-term strength

Long-term strength is an important index of the long-term stability and safety of engineering applications and is used for analyzing the conditions of accelerated rheological failure. Traditional methods for determining long-term strength include the transition rheological method, isochronal curve method, and steady rheological rate intersection method (Wang et al. 2018; Metzler and Nonnenmacher 2003; Zhou et al. 2014). The isochronal curve method involves complicated data extraction but is based on a clear concept; therefore, this method is adopted in this paper. The axial strains and generalized shear stresses (q) at $t = 5.042, 10.084, 15.126, 20.168, 23.109, 30.252, 40.336,$ and 50 h were extracted, as shown in Fig. 4. The generalized shear stress (q) can be calculated using Eq. (1).

$$q = \frac{1}{\sqrt{2}} \sqrt{(\sigma_1 - \sigma_2)^2 + (\sigma_2 - \sigma_3)^2 + (\sigma_3 - \sigma_1)^2} = \sqrt{3J_2} \quad (1)$$

According to the loading stress path mentioned above, q is 18.1, 37.7, 58.4, 79.4, 99.8, and 120.9 kPa, respectively. The creep process of soft clay exhibits nonlinear deformation characteristics; larger axial stresses and longer loading times lead to greater nonlinear characteristics. The isochronal stress-strain curve of soft clay changes approximately linearly when q is less than 79.4 kPa. The stress vs. strain isochronal curve presents a significant inflection point when q is greater than 79.4 kPa; therefore, the long-term strength (σ_∞) of soft clay is 79.4 kPa.

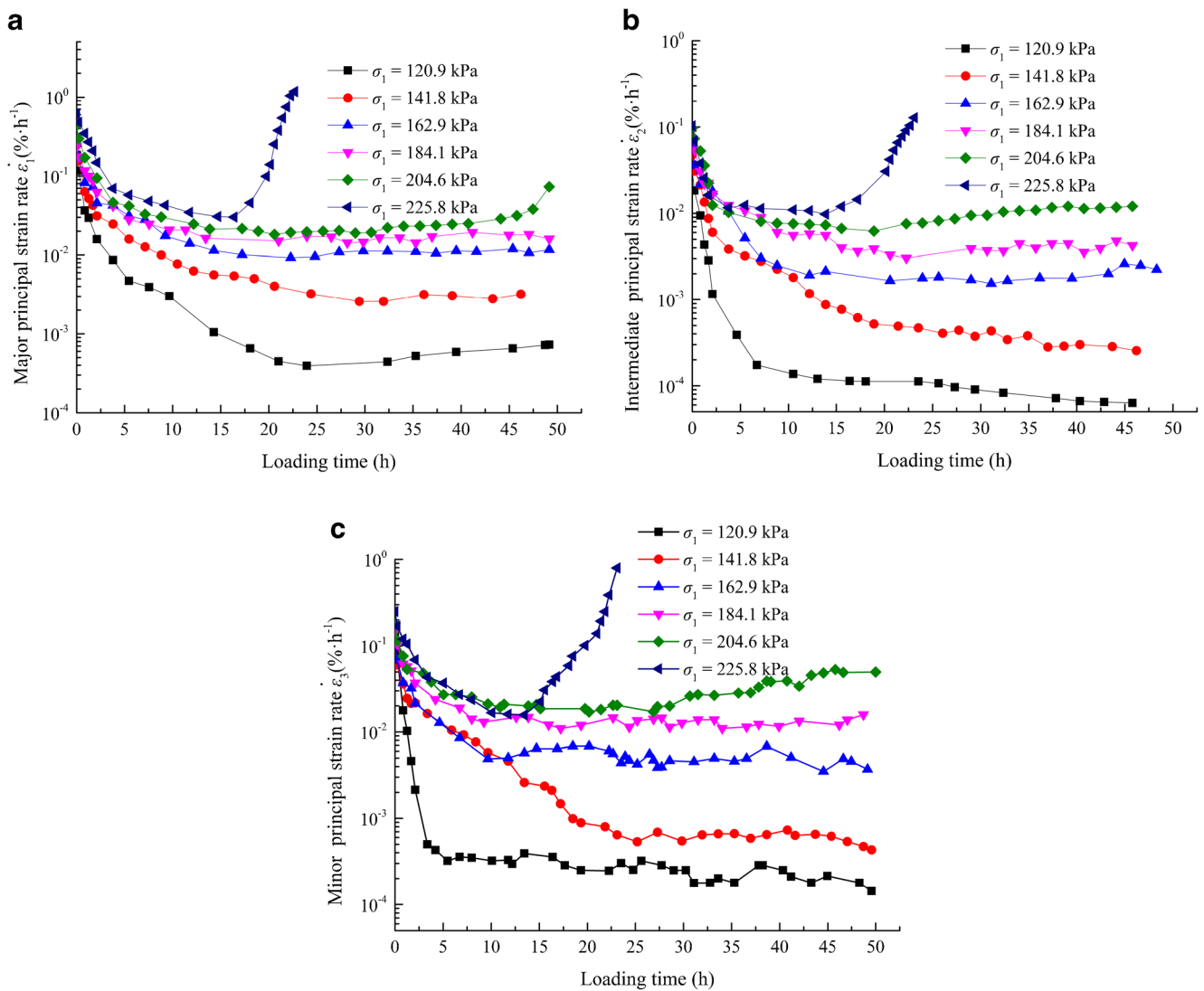


Fig. 3 Strain rate results for a $\dot{\epsilon}_1$, b $\dot{\epsilon}_2$, and c $\dot{\epsilon}_3$

Prediction of the accelerated creep initiation time

The evolution equation for the creep damage rate of materials, proposed by Kachanov (1992), is used to predict the failure time (t_f) of soft clay under loading by integration of Eq. (2):

$$t_f = \frac{1}{A(1 + \nu)\sigma^\nu}, \tag{2}$$

where σ is the stress corresponding to accelerated creep, i.e., the generalized shear stress; and A and ν are the material constants, which can be obtained by fitting experimental data. The specimen is rapidly damaged after accelerated creep occurs; therefore, it is thought to be more practical to predict the time at which accelerated creep begins. Consequently, the t_f calculated according to Eq. (2), which corresponds to the start of accelerated creep, is 41.60 h and 18.07 h for soft clay when q is 99.8 kPa and 120.9 kPa,

respectively, according to the results of this study. The model parameters $A = 1.27 \times 10^{-11}$ and $\nu = 4.28$ can be obtained by substituting the above data into Eq. (2). Therefore, the start time of accelerated creep for soft clay under different generalized shear stress conditions can be obtained as follows:

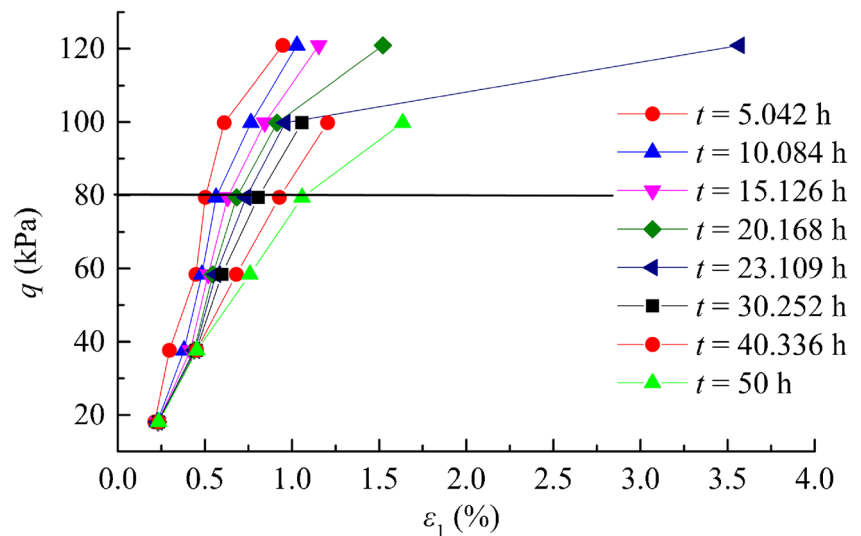
$$t_f = \frac{1}{6.7056 \times 10^{-11} q^{4.28}}. \tag{3}$$

Fractional creep model of soft clay

Fractional calculus theory

The fractional calculus theory can describe derivatives or integrals of any order and thus describes the nonlinear

Fig. 4 Isochronous stress–strain curves of soft clay



deformation characteristics of materials. The main fractional differential operator includes the Riemann–Liouville operator and Caputo operator (Hilfer 2000;

Kilbas and Saïgo 1997). The Riemann–Liouville fractional differential operator is adopted herein, which is expressed as:

$${}^{RL}D_t^\alpha f(t) = \left(\frac{d}{dt}\right)^n I_{a^+}^{n-\alpha} f(t) = \frac{1}{\Gamma(n-\alpha)} \left(\frac{d}{dt}\right)^n \int_a^t \frac{f(\tau) d\tau}{(t-\tau)^{\alpha-n-1}}, (n-1 \leq \alpha < n, t > a). \tag{4}$$

The Riemann–Liouville fractional integral operator can be expressed as:

$$I_a^\alpha f(t) = \frac{1}{\Gamma(\alpha)} \int_a^t \frac{f(\tau) d\tau}{(t-\tau)^{1-\alpha}}, (\alpha > 0, t > a), \tag{5}$$

where $\Gamma(\bullet)$ is the gamma function; D and I are the derivative and integral, respectively; t is the upper limit of the integral; and α is the fractional order.

Fractional creep constitutive model

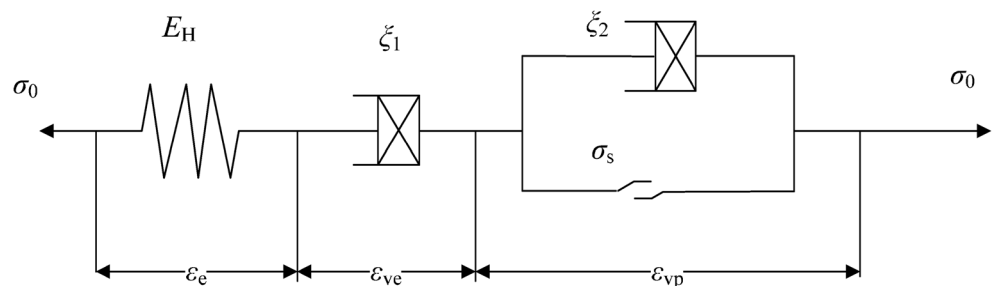
The creep curves of soft clay include instantaneous deformation, deceleration creep, steady creep, and accelerated creep. Moreover, soft clay presents elastic–viscous and elastic–viscoplastic characteristics under constant load

conditions. Therefore, the creep constitutive model of soft clay should include elastic, viscoelastic, and plastic elements.

The Burgers model, which can describe the instantaneous deformation and steady creep, is commonly used in rheological constitutive equations of geotechnical materials. However, this model cannot account for accelerated creep. Therefore, the Burgers model has been improved by using the fractional calculus theory (Pu et al. 2018).

However, the fractional-order Burgers model can only describe the deceleration creep or accelerated creep characteristics of geomaterials. Moreover, it only describes viscous and elastic elements but cannot describe plastic characteristics. Therefore, a FFC model is established to characterize the unsteady creep characteristics of soft clay based on the integer and fractional Burgers models (Fig. 5).

Fig. 5 Four-element fractional-order creep model for soft clay



Hooke’s law is used to characterize the instantaneous elastic deformation of geomaterials, the Abel dashpot connected to a Hookean body is used to characterize the stress vs. strain characteristics of geomaterials between ideal elastomers and ideal fluids, and the element that consists of an Abel dashpot connected in parallel with a friction plate is used to characterize the accelerated creep characteristics of geomaterials.

The viscoplastic strain (ε_{vp}) is 0 if $\sigma < \sigma_s$; however, if $\sigma \geq \sigma_s$, we have

$$\frac{d^{\beta_2} \varepsilon_{vp}(t)}{dt^{\beta_2}} = \frac{\sigma_0 - \sigma_s}{\xi_2} \tag{6}$$

Thus,

$$\varepsilon_{vp}(t) = \frac{\sigma_0 - \sigma_s}{\xi_2} \frac{t^{\beta_2}}{\Gamma(1 + \beta_2)} \quad \beta_2 > 1, \tag{7}$$

where σ_s is the stress threshold for accelerated creep, which is generally taken as the long-term strength (σ_∞) of the material (i.e., $\sigma_s = \sigma_\infty$), and β_2 is the fractional order of the element that consists of the Abel dashpot in parallel with the friction plate for $\beta_2 > 1$.

Thus, the FFC model is represented by:

$$\begin{cases} \varepsilon = \frac{\sigma_0}{E_H} + \frac{\sigma_0}{\xi_1} \frac{t^{\beta_1}}{\Gamma(1 + \beta_1)} & (\beta_1 \leq 1) & \sigma_0 < \sigma_s \\ \varepsilon = \frac{\sigma_0}{E_H} + \frac{\sigma_0}{\xi_1} \frac{t^{\beta_1}}{\Gamma(1 + \beta_1)} + \frac{\sigma_0 - \sigma_s}{\xi_2} \frac{t^{\beta_2}}{\Gamma(1 + \beta_2)} & (\beta_1 \leq 1, \beta_2 > 1) & \sigma_0 \geq \sigma_s \end{cases}, \tag{8}$$

where E_H is the elastic modulus; ξ_1 and ξ_2 are the viscous coefficients of the Abel dashpot, which represent deceleration creep and accelerated creep, respectively; and β_1 and β_2 represent the creep rates of geotechnical materials. In Eq. (8), the first term is time independent and represents instantaneous elastic deformation, and the second term is time dependent and represents steady creep, while $\sigma_0 < \sigma_s$. However, if $\sigma_0 \geq \sigma_s$, the third term represents the accelerated creep process.

Three-dimensional form of the FFC model

The FFC model can describe the creep characteristics of soft clay under uniaxial or triaxial conditions, but cannot consider the effect of the intermediate principal stress (σ_2). Therefore, a 3D model should be developed.

The total strain of the 3D-FFC model can be expressed as:

$$\varepsilon_{ij} = \varepsilon_{ij}^e + \varepsilon_{ij}^{ve} + \varepsilon_{ij}^{vp}, \tag{9}$$

where ε_{ij}^e , ε_{ij}^{ve} , and ε_{ij}^{vp} are the elastic, viscoelastic, and viscoplastic strain tensors, respectively.

The constitutive relationship for a 3D elastomer according to the generalized Hooke’s law is as follows:

$$\varepsilon_{ij}^e = \frac{S_{ij}}{2G_0} + \frac{\sigma_m}{3K} \delta_{ij}, \tag{10}$$

where G_0 and K are the shear modulus and bulk modulus of the Hooke’s body, respectively; σ_m is the spherical stress; S_{ij} is the stress deviatoric tensor; and δ_{ij} is the Kronecker delta. The spherical stress has little effect on the creep properties of soft clay, whereas the stress deviatoric tensor plays a major role in creep (Su et al. 2019). Therefore, the effect of the spherical stress is neglected when calculating the elastic strain tensor, i.e., Eq. (10) is simplified as follows:

$$\varepsilon_{ij}^e = \frac{S_{ij}}{2G_0}. \tag{11}$$

Assuming that the rheological deformation of soft clay is mainly caused by the stress deviatoric tensor, the 3D viscoelastic constitutive relationship of the Abel dashpot is:

$$e_{ij}^{ve}(t) = \frac{S_{ij}}{3\xi_1} \frac{t^{\beta_1}}{\Gamma(1 + \beta_1)}, \tag{12}$$

where e_{ij}^{ve} is the viscoelastic strain deviatoric tensor.

For the viscoplastic term, it is assumed that the β_2 derivative of deviator strain can be expressed as:

$$\frac{d^{\beta_2} e_{ij}^{vp}(t)}{dt^{\beta_2}} = \frac{\langle F \rangle}{\xi_2} \frac{\partial g}{\partial \sigma_{ij}}, \tag{13}$$

where F is the yield function and g is the plastic potential function, which are used for the same correlation flow rule. It is assumed that the yield function satisfies the following form:

$$F = g = \sqrt{J_2} - \sigma_s / \sqrt{3}. \tag{14}$$

Thus,

$$\begin{aligned} \frac{d^{\beta_2} e_{ij}^{vp}(t)}{dt^{\beta_2}} &= \left(\frac{\sqrt{J_2} - \sigma_s / \sqrt{3}}{\xi_2} \right) \frac{\partial (\sqrt{J_2} - \sigma_s / \sqrt{3})}{\partial \sigma_{ij}} \\ &= \frac{\sqrt{2J_2} - \sigma_s}{3\xi_2} = \frac{S_{ij} - S_{ij}^\infty}{3\xi_2}. \end{aligned} \tag{15}$$

Therefore, the viscoplastic strain deviatoric tensor of the element that consists of the Abel dashpot in parallel with the friction plate is as follows:

$$e_{ij}^{vp}(t) = \frac{S_{ij} - S_{ij}^\infty}{3\xi_2} \frac{t^{\beta_2}}{\Gamma(1 + \beta_2)}. \tag{16}$$

The 3D creep equation of the 3D-FFC model can be then obtained by combining Eqs. (11), (12), and (16), as shown in Eq. (17):

$$\left\{ \begin{array}{l} \varepsilon_{ij} = \frac{S_{ij}^0}{2G_0} + \frac{S_{ij}^0}{3\xi_1} \frac{t^{\beta_1}}{\Gamma(1+\beta_1)} \quad (\beta_1 \leq 1) \\ \varepsilon_{ij} = \frac{S_{ij}^0}{2G_0} + \frac{S_{ij}^0}{3\xi_1} \frac{t^{\beta_1}}{\Gamma(1+\beta_1)} + \frac{S_{ij}^0 - S_{ij}^\infty}{3\xi_2} \frac{t^{\beta_2}}{\Gamma(1+\beta_2)} \quad (\beta_1 \leq 1, \beta_2 > 1) \end{array} \right. \quad S_{ij}^0 < S_{ij}^\infty \quad (17)$$

where e_{ij} is the strain deviatoric tensor, S_{ij}^0 is the stress deviatoric tensor, S_{ij}^∞ is the plasticity strength of soft clay for which the long-term strength was used, and $i, j = 1, 2, 3$, where $i = j$ in the true triaxial test.

Sensitivity analysis for the 3D-FFC model parameters

Sensitivity analysis of parameter ξ_1

Stress conditions with three-stage creep characteristics were selected to analyze the ability of the 3D-FFC model to describe the accelerated creep behavior of soft clay, i.e., $\sigma_1 = 204.6$ kPa, $\sigma_2 = 110.5$ kPa, and $\sigma_3 = 100$ kPa. The other parameters were set to $S_{11}^0 = 66.2$ kPa, $S_{11}^\infty = 52.6$ kPa, $G_M = 339.8$ kPa, $\beta_1 = 0.3605$, $\beta_2 = 4.322$, and $\xi_2 = 20.3 \times$

10^6 kPa h^{4.322}. The axial creep curves for different ξ_1 values are obtained from Eq. (17) and shown in Fig. 6a. The values of ξ_1 are 100, 300, 500, and 700 kPa h^{0.3605} for the aforementioned stress conditions, respectively.

Figure 6a shows that creep strain decreases with increasing ξ_1 , but the values of ξ_1 have no significant effect on the shape of the creep curves. However, the creep increment decreases with the same increment values of ξ_1 . For example, the creep strain is 3.616%, 1.585%, 1.179%, and 1.005% corresponding with ξ_1 which is 100, 300, 500, and 700 kPa h^{0.339}, respectively. On the other hand, the creep increment is 2.03, 0.41, and 0.17, which indicates that ξ_1 is sensitive to creep deformation for small ξ_1 values, while for large ξ_1 values, the change of ξ_1 has a little effect on creep deformation.

Sensitivity analysis of accelerated creep (ξ_2)

The creep curves for different ξ_2 values are obtained under the same stress conditions as in the “Sensitivity analysis of parameter ξ_1 ” section, while ξ_1 is 312.4 kPa h^{0.605}. The values of ξ_2 are 2.03×10^5 , 2.03×10^6 , 2.03×10^7 , and $2.03 \times$

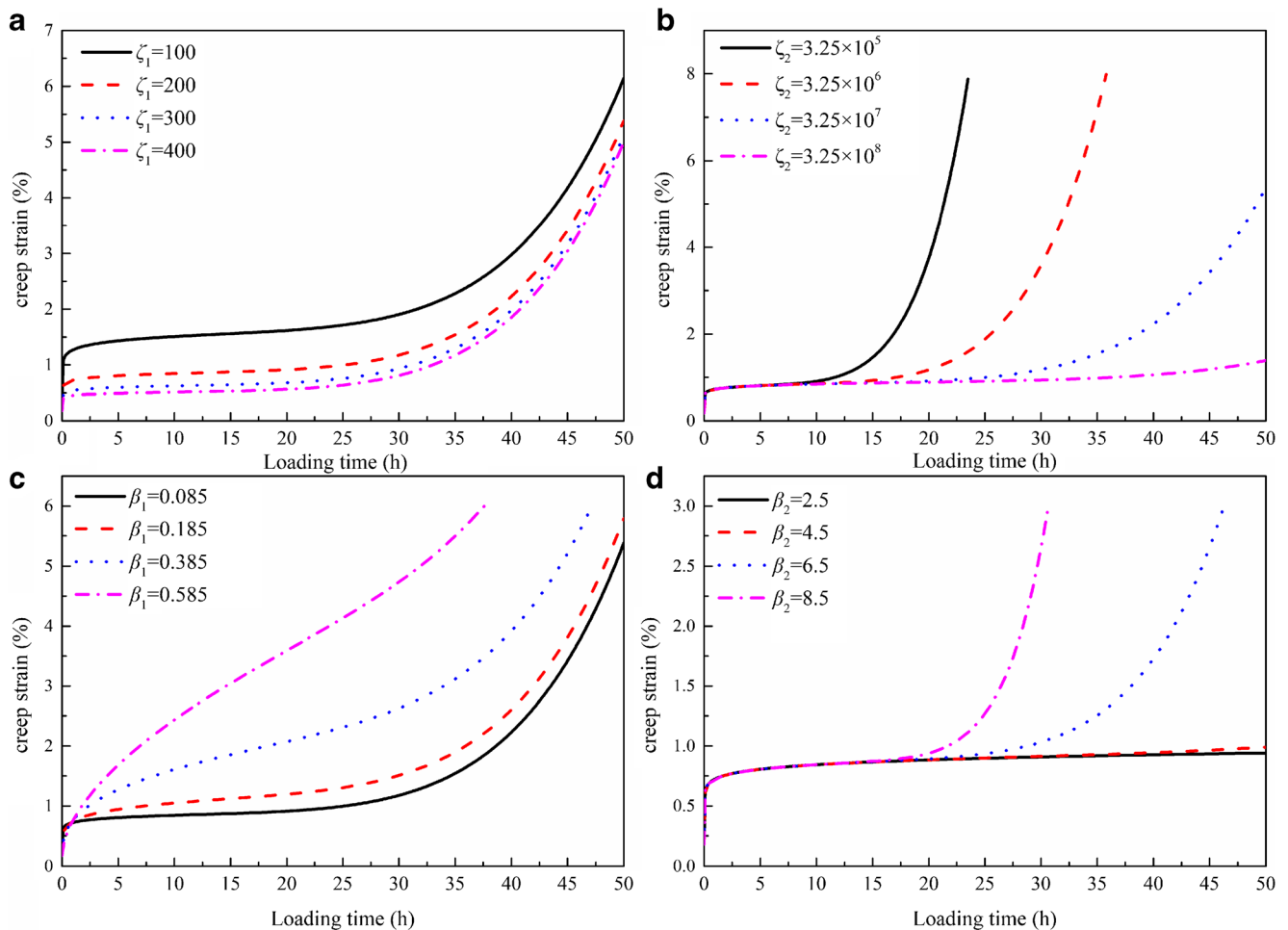


Fig. 6 Creep curves for different values of a ξ_1 , b ξ_2 , c β_1 , and d β_2

$10^8 \text{ kPa h}^{4.322}$, respectively. The axial creep curves for different ξ_2 values are shown in Fig. 6b.

Figure 6b shows that creep deformation decreases with increasing ξ_2 . However, ξ_2 has a significant effect on the shape of the creep curves; the accelerated creep is greater and occurs earlier when the values of ξ_2 are small.

Sensitivity analysis of parameter β_1

The creep curves for different β_1 values are obtained under the same stress conditions as in the “Sensitivity analysis of parameter ξ_1 ” section. When ξ_1 is $312.4 \text{ kPa h}^{\beta_1}$, the values of β_1 are 0.036, 0.136, 0.336, and 0.536, respectively. The axial creep curves for different β_1 values are shown in Fig. 6c.

Figure 6c shows that β_1 has a significant effect on the shape of the creep curves. The steady-state creep duration decreases with increasing β_1 and accelerated creep occurs earlier. The creep curve does not reach a steady state at β_1 values higher than 0.536.

Sensitivity analysis of parameter β_2

The creep curves for different β_2 values are obtained under the same stress conditions as in the “Sensitivity analysis of parameter ξ_1 ” section. When ξ_1 is $312.4 \text{ kPa h}^{\beta_1}$, the values of β_2 are 2.32, 4.32, 6.32, and 8.32, respectively. The axial creep curves for different β_2 values are shown in Fig. 6d.

Figure 6d shows that β_2 also has a significant effect on the shape of the creep curves. As observed for β_1 , the steady-state creep duration decreases with increasing β_2 and accelerated creep occurs earlier. The model’s ability to describe accelerated creep decreases when β_2 is less than 4.32; thus, larger β_2 values can describe the accelerated creep of geomaterials more accurately.

Parameter identification and model verification

Parameter identification

Equation (17) contains five parameters: G_M , β_1 , ξ_1 , β_2 , and ξ_2 . E_1 can be obtained by the ratio of stress to instantaneous strain, and ξ_1 and ξ_2 , which represent the viscous coefficients of the Abel dashpot for deceleration creep and accelerated creep, respectively, can be measured experimentally. However, there is no clear consensus on the best method for determining the viscous coefficients of geotechnical materials. Therefore, the experimental data fitting method is used herein to obtain the values of ξ_1 and ξ_2 . Similarly, β_1 and β_2 are also obtained by experimental data fitting.

The creep model parameters of soft clay (β_1 , ξ_1 , β_2 , and ξ_2) are obtained from the test results under different stress paths,

which are derived by inversion of the rheological formula compiled by MATLAB’s Curve Fitting Toolbox and the Levenberg–Marquardt algorithm (Table 2).

The model parameters change in a regular manner with changing the generalized shear stress states. The model parameter G_M increases with increasing generalized shear stress, whereas β_1 and ξ_1 decrease with increasing generalized shear stress when S_{ij}^0 is smaller than S_{ij}^∞ (the opposite is true when S_{ij}^0 is larger than S_{ij}^∞), and β_2 and ξ_2 increase with increasing generalized shear stress.

Model verification

The creep curves for soft clay can be obtained by substituting the model parameters presented in Table 2 into Eq. (17). The calculated results of the 3D-FFC model are in good agreement with the experimental results (Fig. 7). Therefore, the model not only describes the steady-state creep process of soft clay under low stress states, but also describes the accelerated creep process under high stress states.

Model comparisons

The parameters of the Burgers model and fractional Burgers model are obtained from the experimental results to analyze the accuracy of the 3D-FFC model. The calculated results are compared with the creep test results. As all the

Table 2 Parameters of the 3D four-element fractional-order creep model

	S_{ij}/kPa	G_M/kPa	β_1	$\xi_1/\text{kPa h}^{\beta_1}$	β_2	$\xi_2/\text{GPa h}^{\beta_2}$	R^2
ε_1	10.4	183.2	0.1023	101.7			0.966
	24.4	360.4	0.2431	163.6			0.917
	38.4	235.5	0.3442	303.8			0.974
	52.6	227.9	0.5208	584.6			0.989
	66.2	339.8	0.3605	312.4	4.322	20.3	0.992
ε_2	80.4	402.7	0.3457	233.1	8.257	42.0	0.989
	−0.3	27.26	0.0351	21.6			0.922
	−6.9	417.9	0.2293	267.9			0.918
	−14.0	900.8	0.3500	333.5			0.994
	−21.0	574.5	0.5842	791.1			0.998
ε_3	−27.9	693.5	0.4180	664.7	1.842	0.0193	0.999
	−34.9	982.1	0.3075	457.1	6.404	20.8	0.981
	−10.5	202.1	0.0423	222.0			0.939
	−17.4	285.2	0.2265	202.2			0.901
	−24.5	241.8	0.4811	468.6			0.999
	−31.5	216.9	0.6081	451.2			0.998
	−38.4	214.7	0.4994	418.2	2.163	0.0154	0.997
	−45.4	348.3	0.3560	220.2	6.329	6.90	0.980

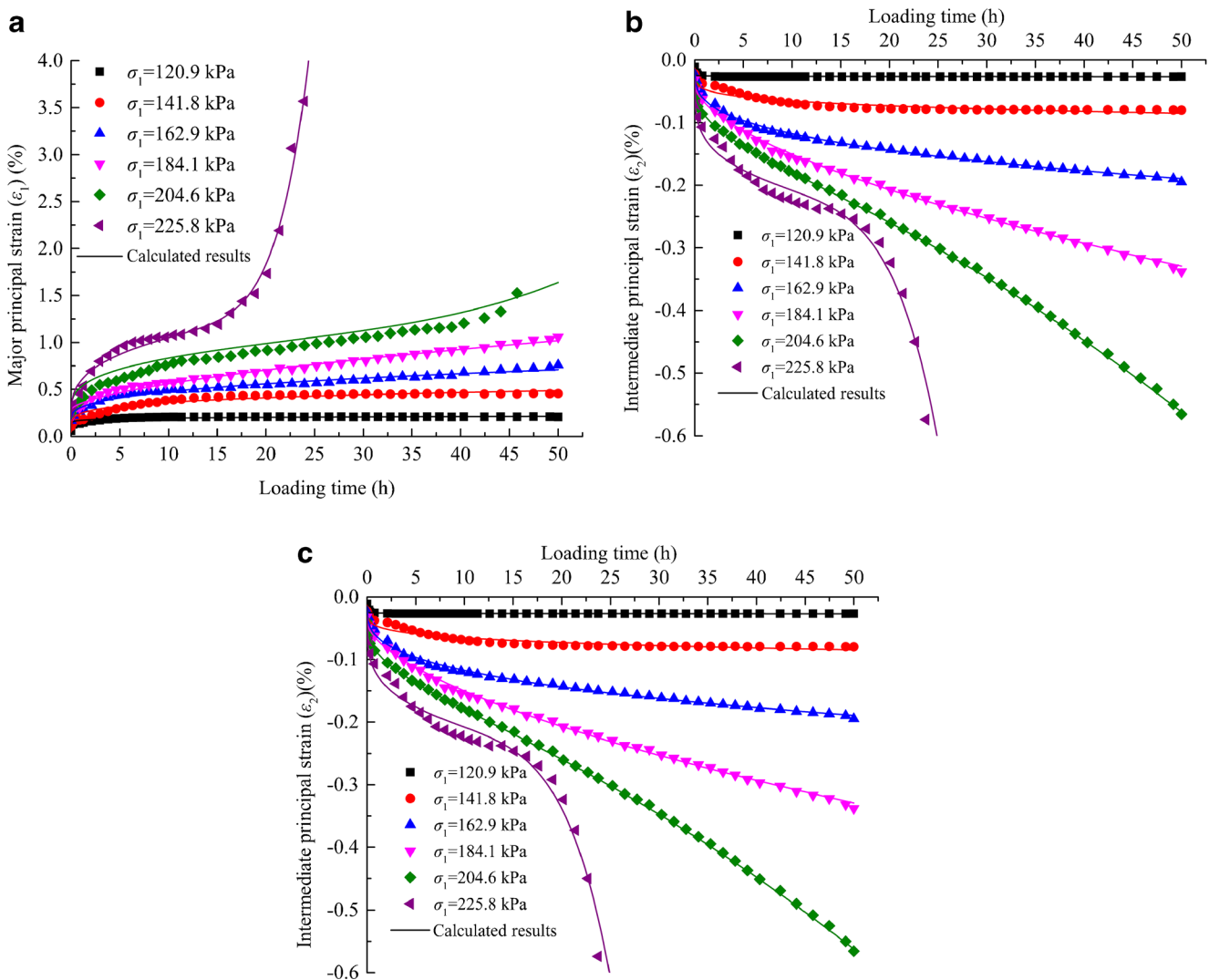


Fig. 7 Comparison of creep curves between model calculated and experimental results: **a** ϵ_{1c} , **b** ϵ_{2c} , and **c** ϵ_{3c}

abovementioned models can describe steady-state creep accurately, therefore, the creep curves for σ_1 values of 204.6 and 225.8 kPa, which are three-stage creep curves, are used to compare the models' performance at describing accelerated creep, as shown in Fig. 8.

Figure 8 shows that the three models exhibit high fitting accuracy when σ_1 is 204.6 kPa; thus, they can adequately describe the deceleration creep, constant creep, and accelerated creep characteristics of soft clay. Soft clay presents clear three-stage creep characteristics when σ_1 is 225.8 kPa. In this stress state, both the fractional Burgers model and the 3D-FFC model can accurately describe the three-stage creep curve of soft clay, whereas the Burgers model cannot. However, the accuracy of the fractional Burgers model gradually decreases in the last stages of the test.

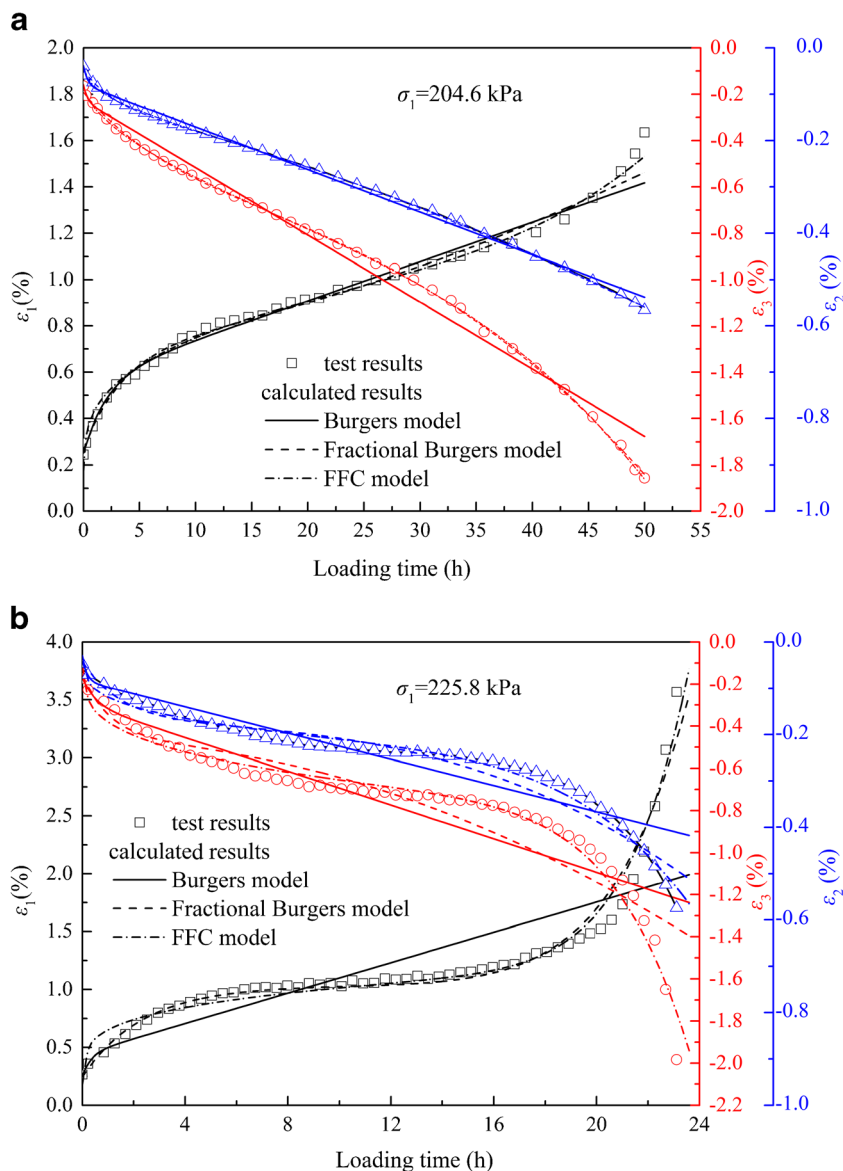
To quantify the differences between the models' calculated results and experimental data, the sum of squared errors (SSE)

and the correlation coefficient (R^2) were calculated. The results of SSE and R^2 calculation under different stress conditions are presented in Tables 3 and 4.

According to Tables 3 and 4, the Burgers model exhibits a larger SSE and smaller R^2 than those of the fractional Burgers model and 3D-FFC model. When σ_1 is 204.6 kPa, the SSE and R^2 values for the Burgers model, fractional Burgers model, and 3D-FFC model are 0.2206, 0.1364, and 0.0652 and 0.9762, 0.9852, and 0.9930, respectively, indicating that the 3D-FFC model can describe the creep curves of soft clay more accurately than the Burgers and fractional Burgers models.

Furthermore, for all models, when σ_1 is 225.8 kPa, the SSE values are larger and the R^2 values are smaller than those when σ_1 is 204.6 kPa under the same conditions. This indicates that the models are less accurate at describing accelerated creep than at describing steady creep. However, the SSE values corresponding to the fractional

Fig. 8 Comparison of creep curves for soft clay calculated by three models. **a** $\sigma_1 = 204.6$ kPa. **b** $\sigma_1 = 225.8$ kPa



Burgers model and the 3D-FFC model are less than 1, while the R^2 values are greater than 0.93, indicating that these models can effectively describe the accelerated creep of soft clay, although the four-element fractional model is better than the fractional Burgers model. As the

four-element fractional-order model features a plastic friction element that can describe the viscoelastic-plastic rheological characteristics of soft clay, this model is sufficiently robust to describe the entire creep curve of soft clay.

Table 3 Sum of squared errors (SSE) and correlation coefficient (R^2) of the calculated results when $\sigma_1 = 204.6$ kPa

Strain	Index	Burgers model	Fractional Burgers model	3D-FFC model
ϵ_1	SSE	0.2206	0.1364	0.0652
	R^2	0.9762	0.9852	0.9930
ϵ_2	SSE	0.00892	0.00088	0.00038
	R^2	0.9959	0.9996	0.9998
ϵ_3	SSE	0.3945	0.0123	0.0025
	R^2	0.982	0.9994	0.9997

Table 4 The sum of squares of errors (SSE) and correlation coefficient (R^2) of $\sigma_1 = 225.8$ kPa

Strain	Index	Burgers model	Fractional Burgers model	3D-FFC model
ε_1	SSE	6.289	0.6021	0.4994
	R^2	0.6489	0.9664	0.9721
ε_2	SSE	0.09427	0.03784	0.0141
	R^2	0.8461	0.9382	0.9770
ε_3	SSE	1.272	0.889	0.1509
	R^2	0.7749	0.9426	0.9733

Conclusions

In this study, true triaxial creep tests were performed to investigate the creep characteristics of soft clay and a 3D four-element fractional-order creep constitutive model (3D-FFC) was established and validated. The following conclusions were drawn:

1. The creep curves of soft clay were obtained under true triaxial stress conditions. The values of ε_1 , ε_2 , and ε_3 were 3.568%, -0.5742%, and 1.983% when the samples failed or reached the failure criteria, respectively. This indicates that the axial deformation was more significant than the lateral deformation. The instantaneous and creep deformation, creep rate, and long-term strength were analyzed, and the Kachanov creep damage rate evolution equation was used to predict the starting point of accelerated creep.
2. The FFC model was established based on the fractional Burgers model and then extended to three dimensions according to the 3D viscoelastic-plastic theory. The sensitivities of the model parameters were analyzed. It was found that creep deformation decreases with the increase of parameters ξ_1 and ξ_2 . However, in contrast with ξ_2 , β_1 , and β_2 , ξ_1 has no significant effect on the shape of the creep curves. The smaller the values of ξ_2 , the more obvious the characteristics of accelerated creep and the earlier the occurrence of accelerated creep. The characteristics of the accelerated creep curve become significant with large values of β_1 and β_2 .
3. The parameters of the 3D-FFC model were obtained. The model calculation results were in good agreement with the experimental results. Moreover, comparison results showed that the 3D-FFC model was more accurate than the fractional Burgers model and Burgers model at describing the entire creep curve of soft clay. Thus, the developed 3D-FFC model is capable of not only describing the steady-state attenuation and constant creep stages of soft clay at low stress values, but also describing the accelerated creep stage at high stress values.

The research results will provide scientific basis for solving creep instability of soft clay engineering under true triaxial stress conditions.

Acknowledgments The authors gratefully acknowledge the helpful comments of the reviewers and also thank Editage (www.editage.cn) for English language editing.

Funding information This research was supported by the State Key Laboratory for Geomechanics and Deep Underground Engineering, China University of Mining & Technology (grant no. SKLGDUEK1914), the State Key Program of National Natural Science of China (grant no. 51734009), the National Natural Science Foundation of China (grant no. 51774166), and the Liaoning Natural Science Foundation Guidance Project (grant no. 20180551162).

References

- Chen JR, Pu H, Xiao C (2015) Research on rheology model of broken mudstone based on the fractional theory. *J China Univ Min Technol* 44(6):996–1001. <https://doi.org/10.13247/j.cnki.jcumat.000418>
- Gupta MBS (1978) Effect of long-term manurial treatment on the rheological behaviour and modes of particle association in natural soil clays. *J Indian Soc Soil Sci* 26(1):76–78
- Kumruzzaman M, Yin JH (2010) Influences of principal stress direction and intermediate principal stress on the stress-strain-strength behaviour of completely decomposed granite. *Can Geotech J* 47(47):164–179. <https://doi.org/10.1139/T09-079>
- Hajime M, Sun DA, Akiteru K, Nobuhiko F, Wataru I (2002) Stress-strain behaviour of unsaturated soil in true triaxial tests. *Can Geotech J* 39(3):608–619. <https://doi.org/10.1139/t02-031>
- Hanyga A (2007) Fractional-order relaxation laws in non-linear viscoelasticity. *Continuum Mech Thermodyn* 19(2):25–36. <https://doi.org/10.1007/s00161-007-0042-0>
- Hao YZ, Wang TH, Wang JJ (2019) Structural properties of unsaturated compacted loess for various sample moisture contents. *Arab J Geosci* 12(8):1–10. <https://doi.org/10.1007/s12517-019-4421-1>
- Hilfer R (2000) Fractional diffusion based on riemann-liouville fractional derivatives. *J Phys Chem B* 104(16):3914–3917
- Isakhanov EA (2000) Investigation of the rheological properties of dense clayey soils. *Soil Mech Foundation Eng* 37(5):145–152. <https://doi.org/10.1023/a:1005256218009>
- Kachanov M (1992) Effective elastic properties of cracked solids: critical review of some basic concepts. *Appl Mech Rev* 45(8):304–335. <https://doi.org/10.1115/1.3119761>
- Kilbas AA, Saïgo M (1997) Fractional integrals and derivatives of the H-function [Russian]. *Dokl Akad Nauk Belarusi* 4:34–39,123
- Kuhn MR, Mitchell JK (1992) Modelling of soil creep with the discrete element method. *Eng Comput* 9(2):277–287. <https://doi.org/10.1108/eb023866>
- Li RD, Yue JC, Zhu CZ, Sun ZY (2013) A nonlinear viscoelastic rheological model of soft soil based on fractional order derivative. *Appl Mech Mater* 438–439:1056–1059. <https://doi.org/10.4028/www.scientific.net/amm.438-439.1056>

- Liu Z, Shao J (2018) Strength behavior, creep failure and permeability change of a tight marble under triaxial compression. *Rock Mech Eng* 50(3):1–13. <https://doi.org/10.1007/s00603-016-1134-6>
- Lv XL, Huang MS, Qian JG (2011) The onset of strain localization in cross-anisotropic soils under true triaxial condition. *Soils Found* 51(4):693–700. <https://doi.org/10.3208/sandf.51.693>
- Mainardi F (2010) *Fractional Calculus and waves in linear viscoelasticity: an introduction to mathematical models*. Imperial College Press, London. https://doi.org/10.1007/978-3-7091-2664-6_7
- Metzler R, Nonnenmacher TF (2003) Fractional relaxation processes and fractional rheological models for the description of a class of viscoelastic materials. *Int J Plast* 19(7):941–959. [https://doi.org/10.1016/s0749-6419\(02\)00087-6](https://doi.org/10.1016/s0749-6419(02)00087-6)
- Morsy MM, Chan DH, Morgenstern NR (1995) An effective stress model for creep of clay. *Can Geotech J* 32(5):819–834. <https://doi.org/10.1139/t95-079>
- Nadimi S, Shahriar K (2014) Experimental creep tests and prediction of long-term creep behavior of grouting material. *Arab J Geosci* 7(8):3251–3257. <https://doi.org/10.1007/s12517-013-0920-7>
- Pu SY, Huang ZH, Rao JY, Mu R, Zheng HC, Wang TL, Liu XL, Li W, Wang YH (2018) Fractional-order burgers constitutive model for rock under low dynamic stress. *J Yangtze River Sci Res Instit* 35(2):109–115. <https://doi.org/10.11988/ckyyb>
- Salimi MJ, Lashkari A (2020) Undrained true triaxial response of initially anisotropic particulate assemblies using CFM-DEM. *Comput Geotech* 124:1–17. <https://doi.org/10.1016/j.compgeo.2020.103509>
- Shao S, Luo AZ (2011) Research on the mechanics characteristics of loess tested by a new true tri-axial apparatus. *Adv Mater Res* 261–263:1714–1718. <https://doi.org/10.4028/www.scientific.net/AMR>
- Shi JG, Shao SJ, Tao H, Xu P (2011) True triaxial tests and strength deformation behaviors of unsaturated soils. *Chin J Geotechn Eng* 33(S1):85–90
- Shi WC, Zhu JG, Zhao ZH, Liu HL (2010) Strength and deformation behaviour of coarse-grained soil by true triaxial tests. *J Cent S Univ Technol* 05:1095–1102. <https://doi.org/10.1007/s11771-010-0602-5>
- Shi WC, Zhu JG, Dai GZ, Li XW (2015) True triaxial tests of coarse-grained soil on π -plane and its strength criterion. *J Hohai Univ* 43(1):11–15. <https://doi.org/10.3876/j.issn.1000-1980.2015.01.003>
- Su T, Zhou HW, Zhao JW, Che J, Sun XT, Wang L (2019) A creep model of rock based on variable order fractional derivative. *Chin J Rock Mech Eng* 38(7):1355–1363. <https://doi.org/10.13722/j.cnki.jrme.2018.1382>
- Sun Y, Cheng C (2018) Fractional order creep model for coral sand. *Mechan Time-Dependent Mater* 23:465–476. <https://doi.org/10.1007/s11043-018-9400-5>
- Wang JB, Liu XR, Sun ZP, Zhao BY, Jiang B, Huang TZ (2018) A whole process creeping model of salt rock under uniaxial compression based on inverse S function. *Chin J Rock Mech Eng* 37(11):2446–2459. <https://doi.org/10.13722/j.cnki.jrme.2018.0670>
- Wang YK, Guo L, Gao YF, Qiu Y, Hu XQ, Zhang Y (2016) Anisotropic drained deformation behavior and shear strength of natural soft marine clay. *Mar Georesour Geotechnol* 34(5):493–502. <https://doi.org/10.1080/1064119X.2015.1081653>
- Wu F, Liu J, Bian Y, Zhou Z (2014) Fractional derivative creep model of salt rock. *J Sichuan Univ* 46(5):22–27
- Xu HY, Jiang XY (2017) Creep constitutive models for viscoelastic materials based on fractional derivatives. *Comput Math Appl* 73(6):1377–1384. <https://doi.org/10.1016/j.camwa.2016.05.002>
- Xu YH, Cai M, Zhang XW, Feng XT (2017) Effect of end effect on rock strength in true triaxial compression. *Can Geotech J* 54(6):862–800. <https://doi.org/10.1139/cgj-2016-0393>
- Yin JH, Zhu JG, Graham J (2002) A new elastic viscoplastic model for time-dependent behaviour of normally and overconsolidated clays: theory and verification. *Can Geotech J* 39(1):157–173. <https://doi.org/10.1139/t01-074>
- Zhan ML, Qian JH, Chen XL (1993) Tests on rheological behavior of soft clay and rheologic model. *Chin J Geotech Eng* 15(3):54–62
- Zhao MH, Xiao Y, Chen CF (2004) Laboratory experiment of the rheological property of soft clay and the improved Xiyuan model. *J Hunan Univ* 31(1):48–51 CNKI:SUN:HNDX.0.2004-01-013
- Zheng X, Wen C (2013) A fractional-order model on new experiments of linear viscoelastic creep of Hami melon. *Comput Math Appl* 66(5):677–681. <https://doi.org/10.1016/j.camwa.2013.01.033>
- Zhou H, Wang C, Han B, Duan Z (2011) A creep constitutive model for salt rock based on fractional derivatives. *Int J Rock Mech Min Sci* 48(1):116–121. <https://doi.org/10.1016/j.ijmms.2010.11.004>
- Zhou XP, Shou YD, Qian QH, Yu MH (2014) Three-dimensional nonlinear strength criterion for rock-like materials based on the micromechanical method. *Int J Rock Mech Min Sci* 72:54–60. <https://doi.org/10.1016/j.ijmms.2014.08.013>